

Examination of scaling of Hanbury-Brown–Twiss radii with charged particle multiplicity

Gunnar Gräf* and Marcus Bleicher

*Institut für Theoretische Physik, Goethe Universität Frankfurt, Germany and
Frankfurt Institute for Advanced Studies (FIAS), Ruth-Moufang-Strasse 1, 60438 Frankfurt, Germany*

Qingfeng Li

School of Science, Huzhou Teachers College, Huzhou 313000, China

(Received 1 March 2012; published 2 April 2012)

In the light of the recent Large Hadron Collider data on proton-proton and lead-lead collisions, we examine the question of the multiplicity scaling of Hanbury-Brown–Twiss (HBT) radii in relativistic nuclei and particle interactions. Within the Ultrarelativistic Quantum Molecular Dynamics transport approach we study a large variety of system sizes at different beam energies and extract the HBT radii. In the calculation, we find a good scaling of the radii as a function of charged particle multiplicity, if the change in the multiplicity is caused by a change of centrality at the same energy. However, the scaling is only approximate when the energy, \sqrt{s} , is changed and breaks down when comparing proton-proton to nucleus-nucleus reactions.

DOI: [10.1103/PhysRevC.85.044901](https://doi.org/10.1103/PhysRevC.85.044901)

PACS number(s): 25.75.Ag, 25.75.Gz

I. INTRODUCTION

The properties of strongly interacting matter are described by the theory of quantum chromodynamics (QCD). To explore the details of QCD matter under extreme conditions, one needs to compress and heat up QCD matter to regimes present microseconds after the Big Bang. Today these conditions can only be found in the interior of neutron stars or created in heavy-ion collisions at relativistic energies. Over the past decade the experimental programs at the Super Proton Synchrotron (SPS) (e.g., with the NA49, CERES, and NA50/NA60 experiments) and at the Relativistic Heavy Ion Collider (RHIC) (e.g., PHENIX, STAR, PHOBOS, and BRAHMS) have provided exciting pioneering data on the equation of state, the transport properties of the matter created, and its spatial distributions [1–10]. These programs are currently extended into a system size scan with NA61 at SPS and a systematic beam energy scan (BES) with the RHIC-BES initiative. In addition, at the high-energy frontier, unprecedented data from the Large Hadron Collider (LHC) for (high multiplicity) proton-proton (pp) and Pb + Pb reactions up to $\sqrt{s_{NN}} = 7$ TeV have become available (see Refs. [11,12] for Hanbury-Brown–Twiss [HBT]–related results). Particle correlations (i.e., HBT correlation) or femtoscopy allow deeper insights into the emission patterns and coherence regions of the matter created [13–16]. One generally assumes that the observed HBT radii scale with the charged particle density (or number of participants) as the charged particle density should be a good proxy for the final state volume [17]. However, the interferometry volume may depend not only on multiplicity but also on the initial size of the colliding system [18]. Indeed, one of the surprising LHC results concerns the scaling violation observed in pp reactions as compared to nucleus-nucleus reactions at lower energies at the same charged particle density. In this paper, we explore the spatial structure of the source created in collisions of various heavy ions at different energies

and centralities to shed light on the observed scaling violation when going from pp to AA collisions at the LHC. Other investigations on the charged particle yield scaling can be found in Refs. [5,19–21]. Results for PbPb and pp reactions at the LHC within the same model can be found in Refs. [22,23].

II. MODEL AND HBT CALCULATION

For the present study we employ the Ultrarelativistic Quantum Molecular Dynamics (UrQMD) [24,25] transport model in version 3.3 (for details of version 3.3 see [26,27]). The model can be downloaded from Ref. [28]. For earlier HBT results from UrQMD see Refs. [29–32]. UrQMD is a microscopic nonequilibrium transport model. It models the space-time evolution of nucleus-nucleus collisions from the beginning of the collision until the kinetic freeze-out. Particles are produced via hard collisions, string excitation, and fragmentation and via resonance excitation and decay.

For the calculation of the HBT radii we use the pion freeze-out distribution from UrQMD. Then we calculate the HBT correlation function by [16,17]

$$C(\mathbf{q}, \mathbf{K}) = 1 + \int d^4x \cos(qx) d(x, K), \quad (1)$$

where C is the correlation function, q is the four-momentum distance of the correlated particles, $K = (p_1 + p_2)/2$ is the pair momentum, x is the particle separation four-vector, and d is the normalized pion freeze-out separation distribution, which is an even function of x . For the analysis in this paper all values are taken in the pair longitudinal comoving system (LCMS). Since UrQMD generates a discrete set of freeze-out points, the integral in Eq. (1) is substituted by a sum.

The HBT radii R_{ij} are obtained by fitting the function

$$C(\mathbf{q}, \mathbf{K}) = 1 + \lambda(\mathbf{K}) \exp \left[- \sum_{i,j=0,s,l} q_i q_j R_{ij}^2(\mathbf{K}) \right] \quad (2)$$

to the calculated three-dimensional correlation functions. For the analysis in this paper the correlation functions are

* graef@th.physik.uni-frankfurt.de

fitted over a range $|q_i| < 800$ MeV/c for proton-proton collisions, $|q_i| < 300$ MeV/c for carbon-carbon collisions, and $|q_i| < 150$ MeV/c for all other collisions. The difference in the momentum ranges is motivated by the fact that the width of the peak in the correlation function gets broader for smaller systems. Thus, the fit range is bigger for proton-proton and carbon-carbon than it is for lead-lead collisions.

III. SCALING OF THE HBT RADII

Figure 1 shows the three HBT radii R_{out} , R_{side} , and R_{long} as a function of the charged particle multiplicity at midrapidity ($|\eta| < 1.2$ for pp and $|\eta| < 0.8$ for all other classes), $(dN_{\text{ch}}/d\eta)^{1/3}$, and fixed $k_T = 300\text{--}400$ MeV. The lines with symbols are simulation results for lead-lead collisions at $\sqrt{s} = 2760, 200, 130,$ and 62.4 GeV for 0–5%, 5–20%, 20–50%, and 50–80% centrality, for carbon-carbon at $\sqrt{s} = 200$ GeV in the same centrality classes, for proton-proton at $\sqrt{s} = 7$ TeV with different $dN_{\text{ch}}/d\eta$ classes, for central copper-copper collisions at $\sqrt{s} = 200$ GeV, and for central lead-lead collisions at $E_{\text{lab}} = 158$ GeV. The green stars are experimental results taken from Refs. [1–12]. For nucleus-nucleus reactions one observes a rather linear scaling with $(dN_{\text{ch}}/d\eta)^{1/3}$. The scaling is very

good if the change in $(dN_{\text{ch}}/d\eta)^{1/3}$ is caused by a change of centrality at a fixed energy. However, a small offset on the order of 2–3 fm is visible for different system sizes, if the radii are extrapolated to $N_{\text{ch}} \rightarrow 0$. This is expected due to the finite size of the nuclei in AA reactions [18]. In contrast, increasing the center-of-mass energy leads to a reduction of the radii at a given fixed N_{ch} -bin. The scaling of the source size with $(dN_{\text{ch}}/d\eta)^{1/3}$ for different centralities is a hint that the underlying physics (e.g., pion production via resonance decay versus production via string fragmentation) is nearly unchanged by changes in the collision geometry. A change in \sqrt{s} on the other hand results not only in different weights of the production mechanisms but also in changed expansion dynamics toward a more violent expansion with increased energy. Qualitatively, one expects a scaling of the length of homogeneity as $R = R_{\text{geom}}/\sqrt{1 + \langle v_{\perp}^2 \rangle} m_{\perp}/2T$ [18,33], where R_{geom} is the geometric size of the collision region, v_{\perp} is the transverse flow velocity, and T is the freeze-out temperature. That is, the increase in transverse flow leads to a decrease of the observed radii with increasing energy, as observed in the model. This combination leads to a deviation from the $(dN_{\text{ch}}/d\eta)^{1/3}$ scaling of the HBT radii. The proton-proton calculation (and the data) show significantly smaller radii and a different slope from what is expected from nucleus-nucleus

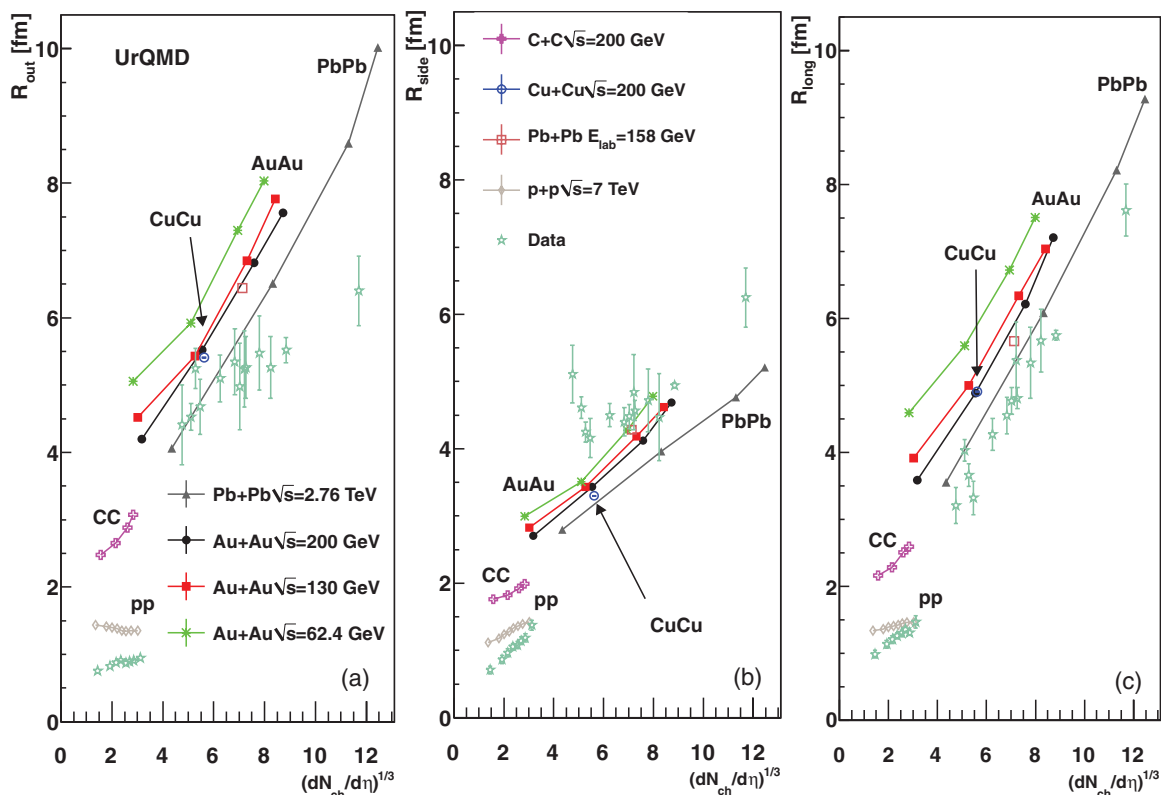


FIG. 1. (Color online) The three HBT radii R_{out} , R_{side} , and R_{long} as functions of the charged particle multiplicity at midrapidity, $(dN_{\text{ch}}/d\eta)^{1/3}$, and fixed $k_T = 300\text{--}400$ MeV. The lines with symbols are the simulation results. The gray triangles, the black circles, the red squares, and the green crosses are for lead-lead collisions at $\sqrt{s} = 2760, 200, 130,$ and 62.4 GeV (in the same order) at 0–5%, 5–20%, 20–50%, and 50–80% centrality for the different points. The pink crosses are results for carbon-carbon at $\sqrt{s} = 200$ GeV for the same centrality classes, and the beige diamonds show results for various multiplicity classes from proton-proton collisions [22]. Blue circles and brown squares depict results for central copper-copper events at $\sqrt{s} = 200$ GeV and central lead-lead collisions at $E_{\text{lab}} = 158$ GeV. The green stars are experimental results for central gold and lead collisions at $k_T = 300$ GeV/c taken from Refs. [1–12].

results. This behavior is attributed to the strongly different particle production mechanisms in AA and pp (i.e., bulk emission vs string or jet dominated emission, which is also in line with the theoretically observed dependence of the HBT radii on the formation time of the hadrons from the jet fragmentation and string decay [22]).

Since the K_{\perp} dependence of the HBT radii tells us much about the expansion of the source [13,15], let us next investigate how a variation of $dN_{\text{ch}}/d\eta$ is reflected in the differential HBT radii as recently discussed in Ref. [34]. Figure 2 shows the three HBT radii R_{out} , R_{side} , and R_{long} at fixed charged particle multiplicity at midrapidity as a function of k_T . The shown calculations are chosen so that they fall roughly into two ($dN_{\text{ch}}/d\eta$) classes. The first class contains calculations with $\langle dN_{\text{ch}}/d\eta \rangle \approx 600$ (exact values are 670 for Pb + Pb at $\sqrt{s} = 2760$ GeV, 20–50% centrality, and 665, 595, and 509 for Pb + Pb at $\sqrt{s} = 200, 130,$ and 62.4 GeV, 0–5% centrality). The second class contains calculations for $\langle dN_{\text{ch}}/d\eta \rangle \approx 25$ (exact values are 23 for C + C at $\sqrt{s} = 200$ GeV, 0–5% centrality, and 32, 28, and 23 for Pb + Pb at $\sqrt{s} = 200, 130,$ and 62.4 GeV and 50–80% centrality).

A very similar slope in K_{\perp} is observed for all UrQMD results. This leads to the conclusion that the observed HBT radii dependence on the radial flow in the model is weaker than observed in the data. The shift in magnitude of the radii is related to the magnitude differences already observed in Fig. 1 that are mainly dominated by geometry and \sqrt{s} effects.

IV. VOLUME AND FREEZE-OUT TIME

Next, let us investigate the energy and system size dependence of the homogeneity volume. Figure 3 shows the volume of homogeneity as a function of $dN_{\text{ch}}/d\eta$ for various systems. Lead-lead calculations are shown for $\sqrt{s} = 2760, 200, 130,$ and 62.4 GeV (grey triangles, black circles, red squares, and green crosses) in the centrality classes 0–5%, 5–20%, 20–40%, and 40–80%. The pink crosses show $\sqrt{s} = 200$ GeV carbon-carbon results for the same centralities, and the beige diamonds represent proton-proton calculations at $\sqrt{s} = 7$ TeV for different $dN_{\text{ch}}/d\eta$ bins. Blue circles and brown squares depict results for central copper-copper

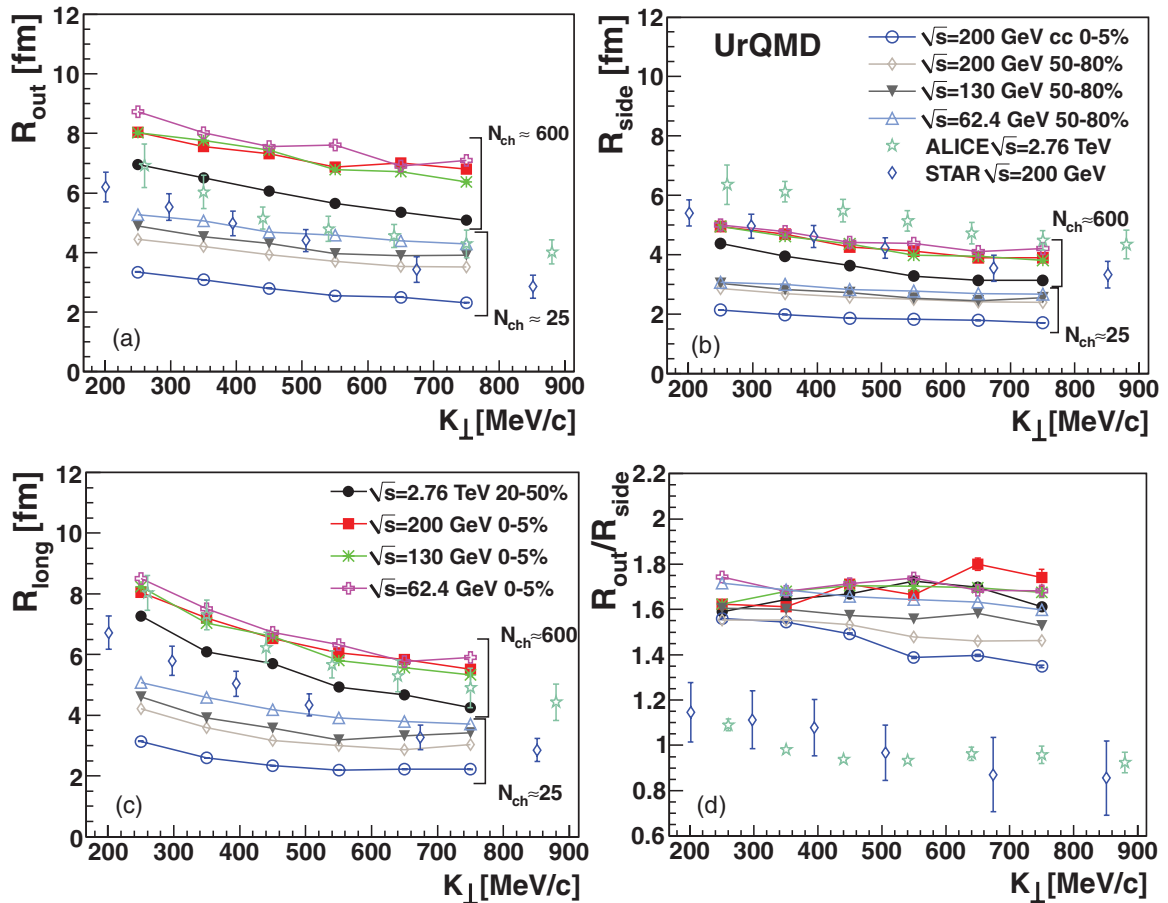


FIG. 2. (Color online) The k_{\perp} dependence of R_{out} , R_{side} , and R_{long} . The black dots are calculations at $\sqrt{s} = 2760$ GeV and 20–50% centrality; the red squares, the green crosses, and the pink crosses are lead-lead for 0–5% centrality at $\sqrt{s} = 200, 130,$ and 62.4 GeV. They have $\langle dN_{\text{ch}}/d\eta \rangle \approx 670, 665, 595,$ and 509 . The other presented calculations are carbon-carbon at $\sqrt{s} = 200$ GeV for 0–5% centrality (blue circles) and lead-lead at $\sqrt{s} = 200, 130,$ and 62.4 GeV (beige diamonds, grey triangles, and blue triangles), all for 50–80% centrality. These collisions have $\langle dN_{\text{ch}}/d\eta \rangle \approx 23, 32, 28,$ and 23 . The green stars represent ALICE lead-lead data for central collisions at $\sqrt{s} = 2760$ GeV [12]. The blue diamonds are experimental results for central gold-gold collisions at $\sqrt{s} = 200$ GeV from the STAR collaboration [1].

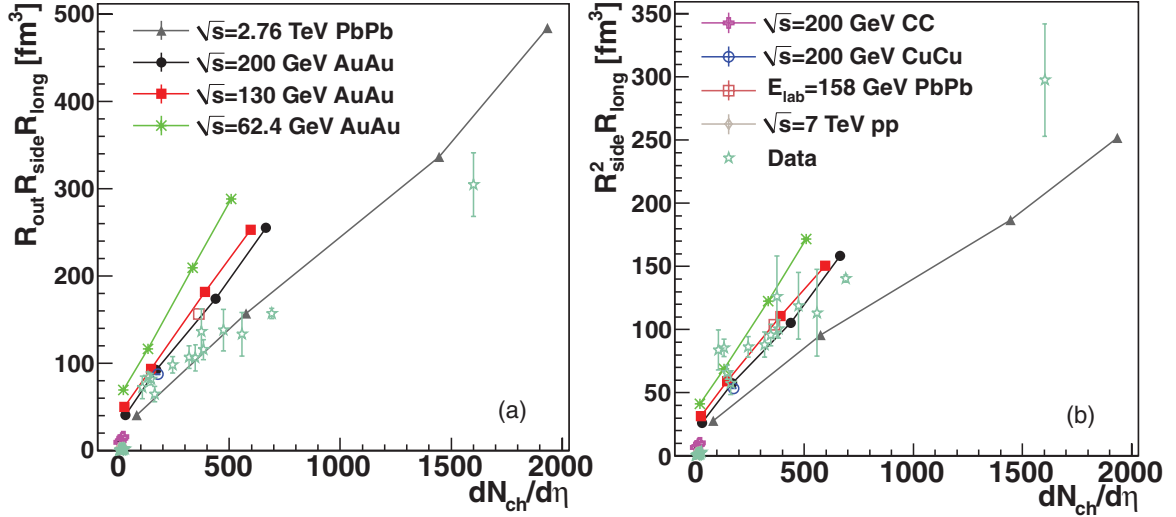


FIG. 3. (Color online) Two definitions of the volume of homogeneity as a function of energy for various systems. In the left plot the volume is defined as $R_{\text{out}} R_{\text{side}} R_{\text{long}}$ and in the right plot the volume is defined as $R_{\text{side}}^2 R_{\text{long}}$. The gray triangles, black circles, red squares, and green crosses depict UrQMD results for lead-lead collisions at (in this order) $\sqrt{s} = 2760, 200, 130,$ and 62.4 GeV for the centralities 0–5%, 5–20%, 20–40%, and 40–80%. The pink crosses are carbon-carbon calculations at $\sqrt{s} = 200$ GeV for the same centralities, the blue circles are central copper-copper collisions at $\sqrt{s} = 200$ GeV, and the brown squares are central lead-lead collisions at $E_{\text{lab}} = 158$ A GeV. The beige diamonds depict proton-proton results at $\sqrt{s} = 7$ TeV for different $(dN_{\text{ch}}/d\eta)^{1/3}$ classes. The green stars show experimental results taken from Refs. [1–12].

events at $\sqrt{s} = 200$ GeV and central lead-lead events at $E_{\text{lab}} = 158$ GeV. These results are compared to experimental data [1–12], which are represented by green stars. In line with the experimental data, a strong increase in the volume proportional to the charged particle multiplicity is observed. A good agreement between experiment and theory is observed for the quantity $R_{\text{side}}^2 R_{\text{long}}$ while the experimental results for $R_{\text{out}} R_{\text{side}} R_{\text{long}}$ are slightly overestimated. This is due to R_{out} that is too large in the calculations. The overestimation of R_{out} is common for hadronic cascade models and can be explained by a lack of pressure in the early stage of the heavy-ion collision [30,35]. While the volume of the homogeneity region for each individual energy scales very well with $dN_{\text{ch}}/d\eta$ Fig. 3 shows a steeper slope with decreasing energy. The calculations also hint to an offset for AA reactions on the order of 25 fm^3 ($R_{\text{side}}^2 R_{\text{long}}$) and 50 fm^3 ($R_{\text{out}} R_{\text{side}} R_{\text{long}}$).

Finally, we explore the apparent freeze-out times τ_f . The results are obtained by fitting the hydrodynamically motivated Eq. (3) [12,36] to the k_{\perp} dependence of R_{long} in the interval $K_{\perp} = 200\text{--}800$ MeV/c. For this purpose the pion freeze-out temperature is assumed to be $T = 120$ MeV:

$$R_{\text{long}}^2 = \tau_f^2 \frac{T}{m_{\perp}} \frac{K_2(m_{\perp}/T)}{K_1(m_{\perp}/T)}, \quad (3)$$

where $m_{\perp} = \sqrt{m_{\pi}^2 + k_{\perp}^2}$ and K_i are the integer order modified Bessel functions. Figure 4 shows the freeze-out time as a function of $dN_{\text{ch}}/d\eta$ for various systems. The grey triangles, the black circles, the red squares, and the green crosses are calculations of lead-lead collisions at $\sqrt{s} = 2760, 200, 130,$ and 62.4 GeV (in the same order) for the centralities 0–5%, 5–20%, 20–40%, and 40–80%. The pink crosses are carbon-carbon collisions at $\sqrt{s} = 200$ GeV for the same centralities. The blue circles are calculations for central copper-copper

collisions at $\sqrt{s} = 200$ GeV and central lead-lead collisions at $E_{\text{lab}} = 158$ A GeV. Experimental results [1–10,12] are depicted by green stars. As for all the other observables, there is scaling for each energy individually. As anticipated from the calculations of R_{long} the decoupling time τ_f increases with decreasing energy. This confirms the idea of a shorter

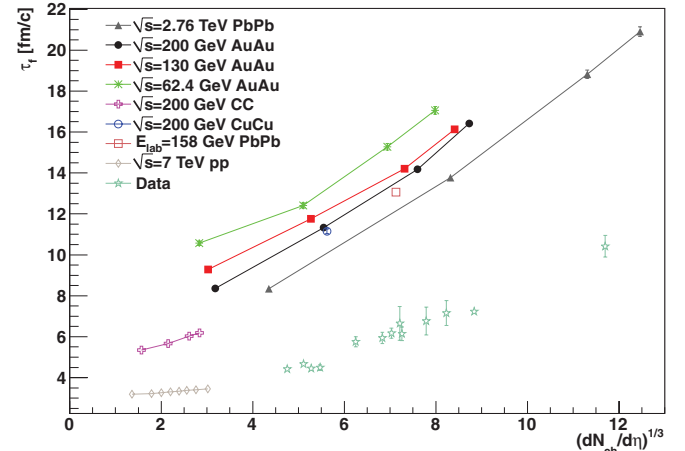


FIG. 4. (Color online) The freeze-out time as a function of energy for various systems. The grey triangles, black circles, red squares, and green crosses depict UrQMD results for lead-lead collisions at (in this order) $\sqrt{s} = 2760, 200, 130,$ and 62.4 GeV for the centralities 0–5%, 5–20%, 20–40%, and 40–80%. The pink crosses are carbon-carbon calculations at $\sqrt{s} = 200$ GeV for the same centralities, the blue circles are central copper-copper collisions at $\sqrt{s} = 200$ GeV, and the brown squares are central lead-lead collisions at $E_{\text{lab}} = 158$ A GeV. The beige diamonds depict proton-proton results at $\sqrt{s} = 7$ TeV for different $(dN_{\text{ch}}/d\eta)^{1/3}$ classes. The green stars show experimental results taken from Refs. [1–10,12].

decoupling time with increased energy. The offset in τ_f for $dN_{\text{ch}}/d\eta \rightarrow 0$ seems to hint at a minimal decoupling time $\tau_f^{\text{min}} \sim 4\text{--}8$ fm/c in AA reactions and $\tau_f^{\text{min}} < 2$ fm/c in pp .

V. SUMMARY AND OUTLOOK

In the light of recent LHC data on pp and AA collisions, which indicate a modification of the multiplicity scaling of the HBT radii, we have explored the N_{ch} scaling for a large variety of systems and energies. We find good scaling of the radii with $dN_{\text{ch}}/d\eta$ within a given system and energy. While the radii decrease slightly with increasing beam energy, they have a similar slope when plotted versus $(dN_{\text{ch}}/d\eta)^{1/3}$ at all energies. When analyzing the freeze-out volume versus $dN_{\text{ch}}/d\eta$ the increasing steepness of the slope for decreasing energies becomes visible. For all observables the scaling

of the results for pp collisions differ strongly from the nucleus-nucleus results. We relate this observation to the different particle emission patterns (bulk vs strings) in AA and pp .

ACKNOWLEDGMENTS

This work was supported by the Helmholtz International Center for FAIR within the framework of the LOEWE program launched by the State of Hesse, GSI, and BMBF. G.G. thanks the Helmholtz Research School for Quark Matter Studies for support. Q.L. thanks the key project of the Ministry of Education (No. 209053), the NNSF (No. 10905021 and No. 10979023), the Zhejiang Provincial NSF (No. Y6090210), and the Qian-Jiang Talents Project of Zhejiang Province (No. 2010R10102) of China for financial support.

-
- [1] J. Adams *et al.* (STAR Collaboration), *Phys. Rev. C* **71**, 044906 (2005).
 - [2] M. A. Lisa *et al.* (E895 Collaboration), *Phys. Rev. Lett.* **84**, 2798 (2000).
 - [3] C. Alt *et al.* (NA49 Collaboration), *Phys. Rev. C* **77**, 064908 (2008).
 - [4] S. V. Afanasiev *et al.* (NA49 Collaboration), *Phys. Rev. C* **66**, 054902 (2002).
 - [5] D. Adamová *et al.* (CERES Collaboration), *Nucl. Phys. A* **714**, 124 (2003).
 - [6] B. I. Abelev *et al.* (STAR Collaboration), *Phys. Rev. C* **80**, 024905 (2009).
 - [7] B. B. Back *et al.* (PHOBOS Collaboration), *Phys. Rev. C* **73**, 031901 (2006).
 - [8] B. B. Back *et al.* (PHOBOS Collaboration), *Phys. Rev. C* **74**, 021901 (2006).
 - [9] B. B. Back *et al.* (PHOBOS Collaboration), *Phys. Rev. Lett.* **91**, 052303 (2003).
 - [10] B. I. Abelev *et al.* (STAR Collaboration), *Phys. Rev. C* **79**, 034909 (2009).
 - [11] K. Aamodt *et al.* (ALICE Collaboration), [arXiv:1101.3665](https://arxiv.org/abs/1101.3665) [hep-ex].
 - [12] K. Aamodt *et al.* (ALICE Collaboration), *Phys. Lett. B* **696**, 328 (2011).
 - [13] S. Pratt, *Phys. Rev. Lett.* **53**, 1219 (1984).
 - [14] Y. M. Sinyukov, *Nucl. Phys. A* **498**, 151C (1989).
 - [15] Y. Hama and S. S. Padula, *Phys. Rev. D* **37**, 3237 (1988).
 - [16] U. A. Wiedemann and U. W. Heinz, *Phys. Rep.* **319**, 145 (1999).
 - [17] M. A. Lisa, S. Pratt, R. Soltz, and U. Wiedemann, *Annu. Rev. Nucl. Part. Sci.* **55**, 357 (2005).
 - [18] Y. M. Sinyukov and I. A. Karpenko, *Phys. Part. Nucl. Lett.* **8**, 896 (2011).
 - [19] D. Adamova *et al.* (CERES Collaboration), *Phys. Rev. Lett.* **90**, 022301 (2003).
 - [20] S. V. Akkelin and Y. M. Sinyukov, *Phys. Rev. C* **70**, 064901 (2004).
 - [21] S. V. Akkelin and Y. M. Sinyukov, *Phys. Rev. C* **73**, 034908 (2006).
 - [22] G. Graef, Q. Li, and M. Bleicher, [arXiv:1203.4421](https://arxiv.org/abs/1203.4421) [nucl-th].
 - [23] Q. Li, G. Graef, and M. Bleicher, [arXiv:1203.4104](https://arxiv.org/abs/1203.4104) [nucl-th].
 - [24] S. A. Bass, M. Belkacem, M. Bleicher, M. Brandstetter, L. Bravina, C. Ernst, L. Gerland, M. Hofmann *et al.*, *Prog. Part. Nucl. Phys.* **41**, 255 (1998).
 - [25] M. Bleicher, E. Zabrodin, C. Spieles, S. A. Bass, C. Ernst, S. Soff, L. Bravina, M. Belkacem *et al.*, *J. Phys. G* **25**, 1859 (1999).
 - [26] H. Petersen, M. Bleicher, S. A. Bass, and H. Stoecker, [arXiv:0805.0567](https://arxiv.org/abs/0805.0567) [hep-ph].
 - [27] H. Petersen, J. Steinheimer, G. Burau, M. Bleicher, and H. Stoecker, *Phys. Rev. C* **78**, 044901 (2008).
 - [28] Download the most recent UrQMD source code from [<http://urqmd.org/>].
 - [29] Q. Li, M. Bleicher, and H. Stoecker, *Phys. Rev. C* **73**, 064908 (2006).
 - [30] Q. Li, M. Bleicher, and H. Stoecker, *Phys. Lett. B* **659**, 525 (2008).
 - [31] Q. Li, J. Steinheimer, H. Petersen, M. Bleicher, and H. Stoecker, *Phys. Lett. B* **674**, 111 (2009).
 - [32] Q. Li, M. Bleicher, and H. Stoecker, *Phys. Lett. B* **663**, 395 (2008).
 - [33] S. V. Akkelin and Y. M. Sinyukov, *Phys. Lett. B* **356**, 525 (1995).
 - [34] D. Truesdale and T. J. Humanic, *J. Phys. G* **39**, 015011 (2012).
 - [35] S. Pratt, *Nucl. Phys. A* **830**, 51C (2009).
 - [36] A. N. Makhlin and Y. M. Sinyukov, *Z. Phys. C* **39**, 69 (1988).